# A Control Strategy for a Distributed Generation Unit in Grid-Connected and Autonomous Modes of Operation

Fang Gao, *Student Member, IEEE*, and M. Reza Iravani, *Fellow, IEEE*

***Abstract*—This paper presents a new voltage control strategy for an electronically-interfaced distribution generation (DG) unit that utilizes a voltage-sourced converter (VSC) as the interface medium. The control strategy is based on the concept of voltage-controlled VSC (VC-VSC) rather than the conventional current-controlled VSC (CC-VSC). The proposed VC-VSC 1) enables operation of a DG unit in both grid-connected and islanded (autonomous) modes, 2) provides current-limit capability for the VSC during faults, 3) inherently provides an islanding detection method without non-detection zone, 4) provides smooth transition capability between grid-connected and autonomous modes, and 5) can accommodate ride-through capability requirements under a grid-connected mode. This paper also investigates performance of the proposed VC-VSC strategy based on an eigenanalysis in MATLAB, and time-domain simulations in the PSCAD/EMTDC environment.**

***Index Terms*—Autonomous operation, distributed generation (DG), islanding detection, ride-through capability, small-signal analysis, voltage-controlled voltage-sourced converter (VC-VSC).**

## I. Introduction

THE concept of distributed generation (DG) has gained significant acceptance during the last decade [1] due to the 1) high cost of energy, 2) environment concerns, and 3) major advances in DG technologies. Most types of DG units utilize power electronic converters and, in particular, voltage-sourced converter (VSC) units, as the interface media with the utility grid [2], [3]. For a grid-connected DG unit, the interface voltage-source converter (VSC) is conventionally controlled as a current-controlled VSC (CC-VSC) [4]. Thus, direct-quadrature current components of the VSC are used to provide control of instantaneous real- and reactive-power exchange between the VSC and the grid. The VSC synchronization is usually carried by a phase-locked loop (PLL) system, based on voltage signals at the point of common coupling (PCC). The main features of the current-controlled strategy are as follows.

- It provides (almost) independent control of real- and reactive-power components.
- It inherently limits the VSC current during abnormal conditions (e.g., grid faults).

Proliferation of DG units in distribution systems and an increase in the DG depth of penetration [5], [6] indicate that a DG unit is best utilized, if it is capable of:

- operation in a grid-connected mode;
- operation in an islanded or autonomous mode;
- transition between grid-connected and autonomous modes.

In an autonomous (islanded) mode where the frequency and voltage are not dictated by the grid, the conventional current-controlled strategy for the interface VSC is not necessarily the optimum choice. The main reason is that it may result in voltage and/or frequency excursions that lead to either unacceptable operating conditions or instability. To address the problem, the following options can be considered.

- Voltage-controlled VSC (VC-VSC) strategy [7]. Based on this strategy, the VSC provides control over the voltage and frequency at PCC of the DG unit. Drawbacks of this strategy are 1) coupling between instantaneous real- and reactive-power components, and 2) no inherent current-limit capability for the converter during grid faults.
- Hierarchical (VC-VSC and CC-VSC) strategy. This strategy needs provisions for frequency and voltage supervisory control signals to control the PCC frequency and voltage (in an autonomous mode) through the conventional CC-VSC strategy. However, care must be taken to prevent 1) its adverse impact on voltage and/or frequency in the grid-connected mode, 2) dynamic interactions among adjacent DG units and synchronous machines in an autonomous multi-DG grid, and 3) slow dynamic response.
- Hybrid (CC-VSC and VC-VSC) strategy. This approach is based on the transition between CC-VSC and VC-VSC control strategies depending on the mode of operation (i.e., grid-connected or autonomous mode). The main challenge in this approach is a smooth transition between the control strategies which also necessitates fast detection of the change of operating mode.

This paper introduces a novel VC-VSC strategy applicable to both grid-connected and autonomous modes of operation of a DG unit. The proposed strategy enables the DG unit:

- to control its exchanged instantaneous real- and reactive-power components in a grid-connected mode;
- to control voltage and frequency in an autonomous mode.

Other features of the proposed VC-VSC strategy are that it provides 1) current-limit capability for the VSC during transients, 2) an inherent islanding detection approach [8] without

Manuscript received July 7, 2006; revised July 16, 2007. Paper no. TPWRD-00389-2006.

The authors are with the Department of Electrical and Computer Engineering, University of Toronto, Toronto, ON M5S 3G4, Canada (e-mail: gaofang2000@hotmail.com; iravani@ecf.utoronto.ca).

Color versions of one or more of the figures in this paper are available online at http://ieeexplore.ieee.org.

Digital Object Identifier 10.1109/TPWRD.2007.915950

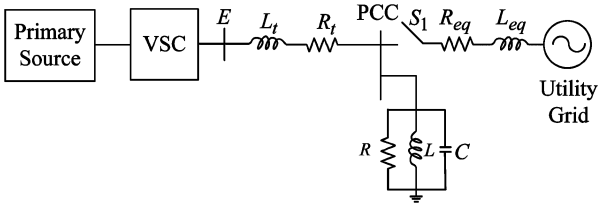


Fig. 1. Single line diagram of the study system.

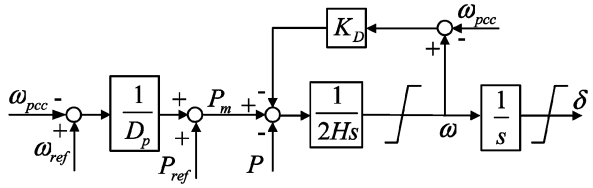


Fig. 2. Block diagram of the proposed frequency control of the VSC-based DG unit of Fig. 1.

nondetection zone (NDZ), 3) smooth transition capability from a grid-connected mode to an autonomous mode, and 4) ease of compliance with ride-through capability requirements in a grid-connected mode [9].

The rest of this paper is arranged as follows. Section II introduces a study system and systematically describes the proposed VC-VSC strategy. Based on an eigenanalysis approach, Section III selects the control parameters and evaluates the dynamic performance of the VC-VSC strategy. Section IV investigates the controller behavior during large-signal transients based on time-domain simulation cases in the EMTDC/PSCAD environment. Section V concludes this paper.

## II. Proposed Control Scheme

To describe the proposed control strategy, the study system of Fig. 1 is considered. The system is composed of a DG unit and a parallel RLC load, and is required to operate either in a grid-connected or an autonomous (islanded) mode when switch $S_1$ is closed or open, respectively. The DG unit includes a primary energy source and a three-phase VSC. The DG unit is interfaced to the point of common coupling (PCC) through a series filter and a transformer which are represented by $L_t$ and $R_t$ (Fig. 1). The local RLC load is connected to the PCC. The main utility grid is represented by an ideal three-phase voltage source and per-phase $R_{eq}$ and $L_{eq}$ components. To describe the concept of the proposed VSC control, and without the loss of generality, we neglect the dynamics of the DG primary source.

### A. Frequency Control

The proposed VSC frequency control is analogous to that of a synchronous machine (SM) (i.e., the VSC instantaneous terminal voltage $E$ is to resemble the internal voltage of an SM [10]). The internal voltage of an SM is aligned with the rotor quadrature-axis and rotates with the rotor speed. Due to the rotor relatively high inertia, the frequency of the space vector of the SM internal voltage cannot have abrupt changes, and exhibits low-frequency variations subsequent to the SM dynamics. Thus, we assume a virtual inertia constant $H$ for the VSC unit of Fig. 1, such that speed $\omega$ of the voltage space vector of the VSC terminal is governed by

$$2H\frac{d\omega}{dt} = P_m - P_{\text{out}} \tag{1}$$

where $P_{\text{out}}$ is the VSC real output power at the PCC and $P_m$ is the VSC input power defined by the droop characteristic

$$P_m - P_{\text{ref}} = \frac{1}{D_p}(\omega_{\text{ref}} - \omega_{pcc}). \tag{2}$$

$\omega_{pcc}$ is the measured frequency at PCC, $D_p$ is the droop constant, and $\omega_{\text{ref}}$ and $P_{\text{ref}}$ are reference values of the converter output frequency and power at the PCC. Considering that the rotating shaft system of an SM is opposed by a viscous damping, (1) can be augmented with the damping term $K_D(\omega - \omega_{PCC})$, thus

$$2H\frac{d\omega}{dt} = P_m - P_{\text{out}} - K_D(\omega - \omega_{pcc}) \tag{3}$$

where $K_D$ is the damping constant. The relationship between the VSC terminal voltage frequency and position $\delta$ is

$$\frac{d\delta}{dt} = \omega. \tag{4}$$

Angle $\delta$ is required for the VSC modulation scheme. The frequency control approach, based on (2)–(4), is represented by the block diagram of Fig. 2.

When the system of Fig. 1 operates in a grid-connected mode (i.e., $S_1$ is closed), $\omega_{\text{PCC}}$ is the same as the frequency of the main grid and is fairly constant. Thus, the virtual governor system of Fig. 2 should set the reference for the output real power and have no impact on the frequency dynamics. In the grid-connected mode, the damping block ensures that the VSC frequency is the same as that of the main grid.

Under an autonomous operating mode of the system of Fig. 1, $\omega_{PCC}$ is the same as the VSC frequency. Thus, the damping block Fig. 2 has no impact on the system dynamics. The frequency dynamics are determined by the droop characteristic. In the case that the autonomous system includes more than one DG unit, the load disturbance can be shared among the DG units based on appropriate droop characteristics.

### B. Voltage Control

The proposed voltage controller for the DG unit of Fig. 1 is shown in Fig. 3. The VSC terminal voltage $E$ is determined by signals $E_1$ and $E_2$. $E_1$ is determined by the voltage droop block

$$E_1 = E_s - D_q Q \tag{5}$$

where $Q$ is the measured output reactive power of the VSC at PCC, $D_q$ is a voltage droop constant, and $E_s$ is the reference value of the VSC terminal voltage. Signal $E_2$ is the output of the reactive power controller and given by

$$E_2 = \frac{K_Q(Q_{\text{ref}} - Q)}{s} \tag{6}$$

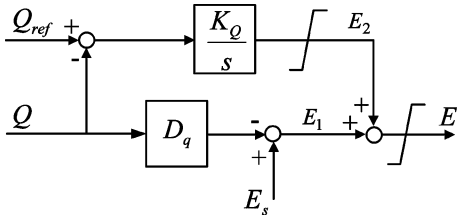


Fig. 3. Block diagram of voltage control of the VSC-based DG unit of Fig. 1.

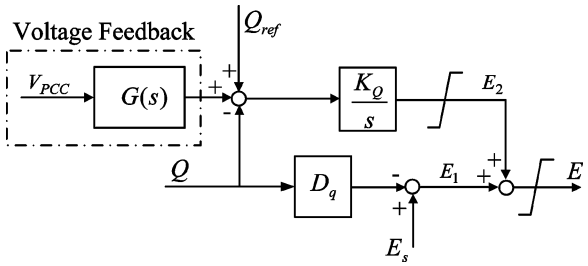


Fig. 4. Block diagram of voltage control with positive feedback of the VSC-based DG unit of Fig. 1.

TABLE I
VOLTAGE LIMITS BASED ON UL1741

| Utility voltage, V (pu) | Maximum time before cessation of operation |
|---|---|
| $V < 0.5$ | 0.16 s |
| $0.5 \le V \le 0.88$ | 2 s |
| $1.1 < V \le 1.2$ | 1 s |
| $V > 1.2$ | 0.16 s |

TABLE II
PARAMETERS OF THE SYSTEM OF FIG. 1

| Parameters | Physical values | Per Unit |
|---|---|---|
| Rated Capacity | $100kVA$ | - |
| Rated Voltage(ll,rms) | $360V$ | - |
| Rated frequency | $60Hz$ | - |
| $L_t$ | $0.35mH$ | 0.1 |
| $R_t$ | $0.026\Omega$ | 0.02 |
| $L$ | $2.76mH$ | 0.8 |
| $C$ | $2.55mF$ | 1.25 |
| $R$ | $1.3\Omega$ | 1 |
| $L_{eq}$ | $0.345mH$ | 0.1 |
| $R_{eq}$ | $0.013\Omega$ | 0.01 |
| $H$ | 0.5s | - |
| $D_p$ | - | 0.05 |
| $D_q$ | - | 0.05 |
| $K_D$ | - | 20 |
| $K_Q$ | - | 10 |
| $T_1$ | 0.159s | - |
| $T_2$ | 0.016s | - |
| $K_V$ | - | 5 |

where $K_Q$ is the integrator gain, and $Q_{\rm ref}$ is the reactive power reference value of the VSC at PCC. Based on Fig. 3, the VSC output voltage $E$ is

$$E = E_1 + E_2 = E_s - D_q Q + \frac{K_Q(Q_{\rm ref} - Q)}{s}. \quad (7)$$

The voltage control objective of a DG unit depends on its operating mode (i.e., grid-connected or autonomous mode). In a grid-connected mode, voltage control is to set the output reactive power of the VSC at PCC. For example, the reference reactive power is set to zero. This objective can be achieved by the control of Fig. 3. However, in an autonomous mode, the DG unit has to supply the load reactive power demand without any reactive power contribution from the main grid. Thus, the reactive power controller (6) of the grid-connected mode is no longer applicable and can drive the system unstable. Therefore, $E_2$ of Fig. 3 is set to zero by imposing $K_Q = 0$ during an autonomous mode and only $E_1$ remains effective. Therefore, the voltage control strategy should change during the transition process from the grid-connected mode to the autonomous mode. This change takes place after islanding is confirmed based on the inherent islanding detection capability of the proposed controller as described in Section II-D.

### C. Over-Current Limiters

A drawback of controlling the VSC of Fig. 1 as a voltage-controlled VSC is that the grid faults and disturbances may subject it to over-currents. To limit over-currents, two dynamic limiters for $\delta$ of Fig. 2 and $E$ of Fig. 3, are introduced. By means of a phase-locked loop (PLL) system, phase angle $\delta_{pcc}$ and amplitude $V_{pcc}$ of the PCC voltage space vector are extracted. The settings of limiters for $\delta$ and $E$ are

$$\delta_{pcc} - \Delta\delta \le \delta \le \delta_{pcc} + \Delta\delta \quad (8)$$

$$V_{pcc} - \Delta E \le E \le V_{pcc} + \Delta E \quad (9)$$

where $\Delta\delta$ and $\Delta E$ are maximum allowable deviations of $\delta$ and $E$ from $\delta_{pcc}$ and $V_{pcc}$, respectively. $\Delta\delta$ and $\Delta E$ are defined based on parameters $L_t$ and $R_t$, and the maximum allowable current of VSC. Limiters for $\omega$ of Fig. 2 and $E_2$ of Fig. 3 affect the over-current indirectly. However, the appropriate selection of these limits can also improve dynamic performance of VSC. The settings for limiters of $\omega$ and $E_2$ are

$$\omega_{\rm ref} - \Delta\omega \le \omega \le \omega_{\rm ref} + \Delta\omega \quad (10)$$

$$-\Delta E_2 \le E_2 \le \Delta E_2 \quad (11)$$

where $[\omega_{\rm ref} - \Delta\omega,\ \omega_{\rm ref} + \Delta\omega]$ is the allowable frequency range of the VSC. $\Delta E_2$ is determined based on parameters $L_t$ and $R_t$, and the allowable reactive power range of the VSC.

### D. Islanding Detection Approach

Reactive power control (i.e., upper path of Fig. 3), which drives the system to an unstable condition during an autonomous mode of operation, also can be exploited for islanding detection. The detection time may exceed and not satisfy the standard requirements [9] if a power exchange between the DG and the grid, prior to the islanding instant, is small. To decrease the detection time, a positive feedback with transfer function $G(s)$, based on the instantaneous PCC voltage, is added to the controller of Fig. 3 as shown in Fig. 4. Transfer function $G(s)$ is given as

$$G(s) = \frac{K_V s}{(1 + T_1 s)(1 + T_2 s)} \quad (12)$$

where $1/T_1$ and $1/T_2$ specify upper and lower corner frequencies. $G(s)$ should 1) ensure that the feedback process is only effective during transients and does not impact the dc steady-state error signal, and 2) provide attenuations for high-frequency

TABLE III
SYSTEM EIGENVALUES

| No. | Eigenvalues | | | Dominant States |
|---|---|---|---|---|
| | Grid-Connected mode | Autonomous mode (with Q control) | Autonomous mode (no Q control) | |
| 1,2 | $-181.3 \pm 1949.4i$ | $-183.0 \pm 1571.6i$ | $-170.5 \pm 1542.4i$ | Electrical states of PCC voltage and branch current |
| 3,4 | $-170.7 \pm 1150.2i$ | $-182.9 \pm 710.5i$ | $-156.2 \pm 708.9i$ | |
| 5,6 | $-3.5 \pm 378.2i$ | $-1.2 \pm 385.9i$ | $-2.9 \pm 387.7i$ | |
| 7,8 | $-30.5 \pm 417.2i$ | - | - | |
| 9 | $-9.3 \pm 43.4i$ | $-19.8$ | $-20.4$ | VSC terminal frequency and angle |
| 10 | | - | - | |
| 11 | $-9.8 \pm 9.0i$ | 0.4 | - | States of reactive power control with voltage feedback |
| 12 | | 26.0 | - | |
| 13 | $-90.0$ | $-97.5$ | - | |

noise. For example, if a two-second islanding detection is required [9], a $1-10$ Hz frequency band for $G(s)$ is selected, and gain $K_V$ is adjusted to achieve the desired islanding detection speed.

In a grid-connected mode of operation, 1) the PCC voltage is dominantly dictated by the grid, and 2) a relatively small reactive-power excursion, imposed by the positive feedback control of Fig. 4, is also absorbed by the grid and does not result in instability.

To ensure ride-through capability of a grid-connected DG unit, the islanding process must be delayed based on the requirements for "maximum time before cessation of operation" of the adopted standard (e.g., Table I corresponding to UL1741 [9]). If the PCC voltage violates the specified limits (e.g., those of Table I), then islanding is confirmed. Otherwise, the islanding detection signal is ignored and the unit continues operation.

Figs. 2 and 4 show that inputs to the proposed VSC control system are: 1) instantaneous real-power and reactive-power components of the VSC at PCC, 2) voltage magnitude and phase angle at PCC, and 3) electrical frequency at the PCC. The voltage phase angle and the frequency signal are obtained from the PCC voltage by means of a PLL system. Other signals are obtained from instantaneous PCC voltage and the VSC current. Thus, the control system of Figs. 2 and 4 is readily implemented.

## III. SMALL-SIGNAL DYNAMIC ANALYSIS

To optimize parameters and demonstrate performance of the proposed controls, a set of small-signal dynamic analysis is performed on the system of Fig. 1. The studies include both autonomous (islanded) and grid-connected modes of operation. A small-signal dynamic model of the grid-connected system is developed in the grid dq frame such that the space vector of the grid voltage source is aligned with the direct-axis. Also a small-signal dynamic model of the autonomous system is developed in the VSC dq frame such that the space vector of the VSC terminal voltage is aligned with the direct-axis. The system parameters are given in Table II.

Table III shows the system eigenvalues corresponding to the 1) grid-connected mode, 2) autonomous mode with reactive power (Q) control, and 3) autonomous mode without reactive power (Q) control. The DG unit supplies 1.0/0.0-p.u. real/reactive-power in the grid-connected mode. When isolated from the main grid, the DG output power depends on the local RLC load demand. Column 5 of Table III identifies the dominant states

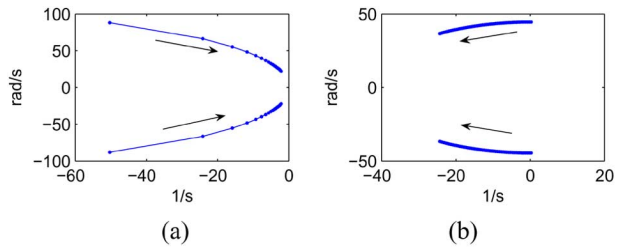


Fig. 5. Trace of eigenpair (9,10) when (a) $H$ changes from 0.1 s to 2 s; (b) $K_D$ changes from 1 to 50.

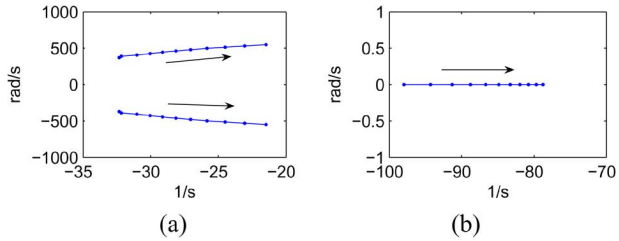


Fig. 6. Trace of (a) eigenpair (7,8) and (b) eigenvalue 13 when $D_q$ changes from 0 to 0.2.

associated with each eigenvalue based on the participation factors. The mode associated with eigenpair (5,6) is dominantly associated with the RLC load.

### A. Small-Signal Dynamics of Grid-Connected Mode

Fig. 5 shows traces of eigenpair (9,10) corresponding to the VSC terminal frequency as functions of parameters of the frequency controller of Fig. 2. As expected, variations of H do not significantly affect the damping of this mode, however, they noticeably change the mode frequency. However, increasing $K_D$ noticeably increases the mode damping, while has insignificant effect on the mode frequency. Thus, H and $K_D$ can be exploited to effectively adjust behavior of the frequency mode.

Variations of $D_q$ of Fig. 4 primarily affect eigenpair (7,8) and eigenvalue 13, Fig. 6. As $D_q$ increases, eigenpair (7,8) and eigenvalue 13 move to the right-hand side. This indicates that a large $D_q$ deteriorates the system behavior in terms of stability. The reason is that the voltage droop characteristic is designed for the autonomous mode and is neither intended nor beneficial for the grid-connected mode.

Variations of $K_Q$ of Fig. 4 also affect eigenpair (7,8) and eigenvalue 13, Fig. 7. As $K_Q$ increases, eigenvalue 13 moves to the left-hand side, but the damping of eigenpair (7,8) decreases.

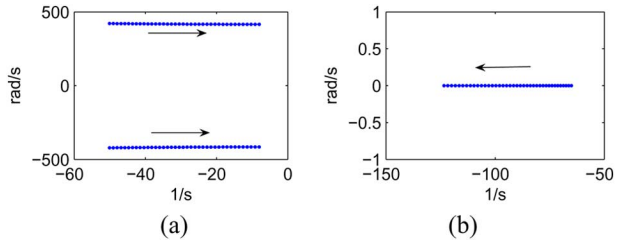


Fig. 7. Impact of increasing $K_Q$ from 1 to 20 on the traces of (a) eigenpair (7,8) and (b) eigenvalue 13.

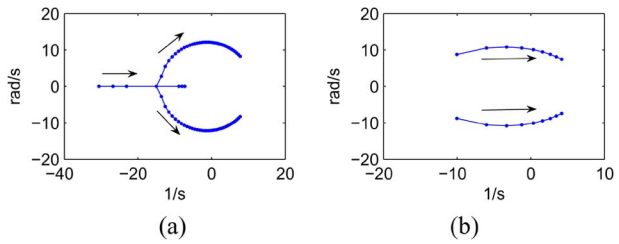


Fig. 8. Trace of eigenpair (11,12) (a) when $K_V$ changes from 1 to 25; (b) when $X_{eq}$ changes from 0.1 to 0.5 p.u., with $X_{eq}/R_{eq} = 5$.

Fig. 8(a) shows a trace of eigenpair (11,12) when $K_V$ is changed from 1 to 25. For small values of $K_V$, between 1 to 4, eigenvalues 11 and 12 are real and located in the left-hand plane. However, as $K_V$ increases beyond 4, eigenvalues 11 and 12 form a conjugate pair and move to the right-hand side, and when $K_V$ exceeds 15, they constitute an unstable oscillatory mode.

Fig. 8(b) shows impact of the grid stiffness on eigenpair (11,12) when $X_{eq}$ is changed from 0.1 to 0.5 p.u. ($X_{eq}/R_{eq} = 5$) and $K_V = 5$. Fig. 8(b) indicates that for a stiff grid (i.e., $SCR \geq 4$), the oscillatory mode associated with eigenpair (11,12) is well damped, however, under non-stiff grid conditions (i.e., $SCR < 4$), the mode can be highly unstable. This instability is due to the reactive power controller of Fig. 4 through the positive feedback signal. Under non-stiff grid conditions, the reactive power disturbance through the positive feedback is not fully absorbed by the grid and results in the system instability.

Fig. 9 shows the effect of the $X_{eq}/R_{eq}$ ratio on eigenpairs (9,10) and (7,8) when the magnitude of network impedance $Z_{eq} = \sqrt{X_{eq}^2 + R_{eq}^2}$ is kept constant at 0.2 p.u. Fig. 9 illustrates that as the ratio $X_{eq}/R_{eq}$ increases from 1 to 20 1) damping of the oscillatory mode associated with eigenpair (7,8) decreases, but the mode always remains stable, 2) however, damping of the mode associated with eigenpair (9,10) increases, and the mode becomes unstable for $X_{eq}/R_{eq} < 1$. The reason for instability is that the controller of Fig. 2 is designed based on the assumption of decoupled P and Q, while P and Q are tightly coupled at low values of $X_{eq}/R_{eq}$. Damping of the mode, even when $X_{eq}/R_{eq}$ is relatively small, can be enhanced based on proper selection of $K_D$ (Fig. 2). The effect of $K_D$ on eigenpair (9,10) is shown in Fig. 5(b).

Eigenanalysis results also reveal that the DG operating point, level of local load, and the amount of power transfer to the grid have an insignificant impact on the system eigenvalues.

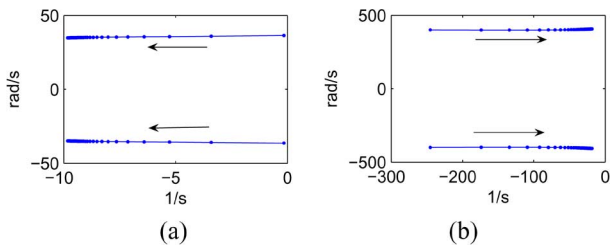


Fig. 9. Trace of eigenpairs (a) (9,10) and (b) (7,8) when $X_{eq}/R_{eq}$ ratio changes from 1 to 20, with constant $Z_{eq} = 0.2$ p.u..

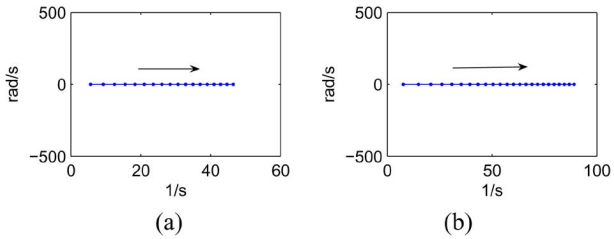


Fig. 10. Trace of eigenvalue 12 when (a) $K_Q$ changes from 1 to 20 ($K_V = 5$); (b) $K_V$ changes from 1 to 25 (($K_Q = 10$).

### B. Small-Signal Dynamics of Autonomous Mode With Q Control of Fig. 4 in Service

In an autonomous mode of operation, when $S_1$ of Fig. 1 is open, 1) eigenpair (7,8) does not exist, and 2) corresponding to the complex conjugate eigenpairs (9,10) and (11,12), three real eigenvalues, as shown in the third column of Table III, exist.

Fig. 10(a) shows that eigenvalue 12, associated with the reactive power controller of Fig. 4, is monotonically unstable, and the instability is more pronounced as $K_Q$ increases. Figs. 7(a) and 10(a) indicate that $K_Q$ can be selected such that 1) in a grid-connected mode, eigenpair (7,8) remains well damped, and 2) in an autonomous mode, eigenvalue 12 exhibits instability as a means for islanding detection.

Fig. 10(b) shows the effect of feedforward gain $K_V$ of Fig. 4 on eigenvalue 12. The comparison of Figs. 8(b) and 10(b) shows that $K_V$ can be selected such that at different values of grid stiffness, eigenpair (11,12) remains stable under the grid-connected mode, and eigenvalue 12 exhibits instability, for islanding detection, during the autonomous mode.

In conformity with the anti-islanding test conditions [9], impacts of load resonant frequency $f = 1/(2\pi\sqrt{LC})$ and load quality factor $q = R\sqrt{C/L}$ on the system eigenvalues are also investigated. The eigenanalysis results show that changing 1) the load resonant frequency within the range of 59.5 Hz to 60.5 Hz while the output real power from the DG unit is zero, and 2) the quality factor q within the range of 1 and 3, introduces no significant impacts on the system eigenvalues, including unstable eigenvalue 12. Since unstable eigenvalue 12 determines the dynamics of the PCC voltage deviations during the islanding detection process, the load resonant frequency and quality factor have no detrimental impacts on islanding detection. This indicates that the islanding detection approach does not have any NDZ in terms of load parameters.

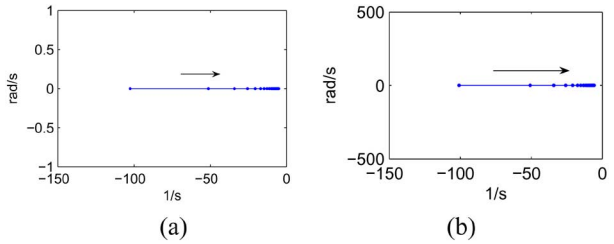


Fig. 11. Trace of eigenvalue 9 when (a) $H$ changes from 0.1 to 2 s; (b) $D_p$ changes from 0.01 to 0.2.

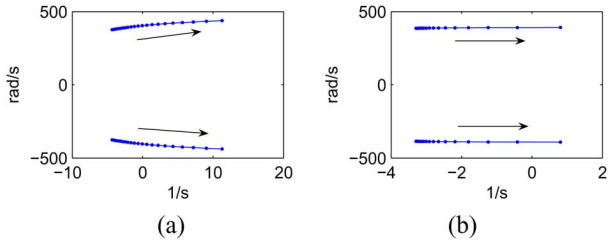


Fig. 12. Trace of eigenpair (5,6) when (a) $D_q$ changes from 0 to 0.2; (b) $C$ changes from 0.5 to 2 p.u. with $L = 0.8$ p.u.

### C. Small-Signal Dynamics of Autonomous Mode With Q Control of Fig. 4 Out of Service

If the system of Fig. 1 is expected to remain operational in an autonomous mode and supply the local load, the reactive power controller, Fig. 4, which drives the system to instability as part of the islanding detection strategy, must be disabled ($K_Q = 0$) subsequent to an islanding event. Disabling the reactive power controller eliminates eigenvalues 11, 12, and 13, Column 4 of Table III. Corresponding to eigenpair (9,10) during the grid-connected mode, only eigenvalue 9 exists during an autonomous mode. Fig. 11 shows impacts of control parameters $H$ and $D_p$ on eigenvalue 9. Fig. 11(a) indicates that increasing $H$ noticeably moves eigenvalue 9 to the right-hand side. Fig. 11(b) shows that as $D_p$ increases, eigenvalue 9 also moves to the right-hand side. This indicates that a large frequency droop has a detrimental effect on the system stability in the autonomous mode.

Fig. 12(a) shows the effect of changing $D_q$ from 0 to 0.2 on the mode associated with eigenpair (5,6). Fig. 12(a) indicates that large values of $D_q$ result in an unstable oscillatory mode. Comparison of Figs. 6(b) and 12(a) indicates that a small $D_q$ (e.g., 0.02) is acceptable.

Fig. 12(b) shows the impact of local reactive load demand on eigenpair (5,6) when capacitor C is changed from 0.5 to 2.0 p.u., while L remains constant. The variation of C changes the load from inductive to capacitive load. As the capacitance increases, the oscillatory mode associated with eigenpair (5,6) moves to the right-half plane. For $C > 1.9$ p.u., the mode becomes unstable. This indicates that for large capacitive loads, voltage droop characteristics should not be used. This is another reason for selecting a small $D_q$, especially under capacitive load conditions. Eigenanalysis results also reveal that the local real load demand does not have a significant impact on the system eigenvalues.

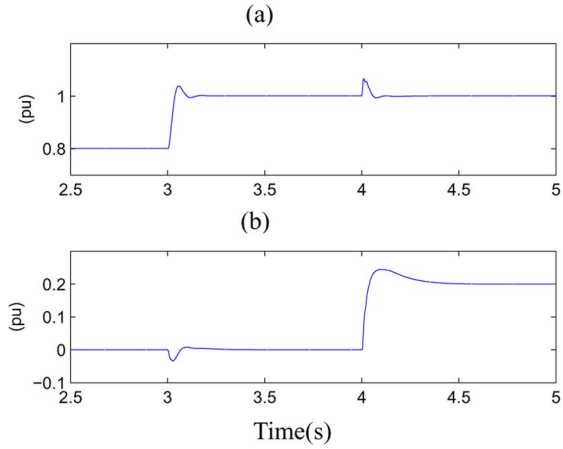


Fig. 13. Response of the DG unit in a grid-connected mode to step changes in references of real and reactive power. (a) DG unit real power at PCC. (b) DG unit reactive power at the PCC.

## IV. Time-Domain Simulation Results

Eigenanalysis of Section III provides a systematic approach to select parameters of the VSC controllers of Figs. 2 and 4. To validate the system performance based on the selected parameters and to illustrate behavior of the system and the controllers due to large-signal transients (e.g., faults and islanding events), a set of time domain simulation studies are conducted on the system of Fig. 1. The EMTDC/PSCAD software package is used as the simulation environment.

### A. Grid-Connected Mode

Fig. 13 shows responses of the controllers of Figs. 2 and 4 under a grid-connected mode of operation. Initially, the system is under a steady-state condition and the DG unit delivers 0.8/0.0 p.u. real/reactive power at PCC. The converter is subjected to step changes in reference values of real/reactive power, at time instants $t = 3.0$ s and $t = 4.0$ s, from 0.8/0.0 to 1.0/0.2 p.u., respectively. Fig. 13(a) and (b) shows variations in real- and reactive-power at the PCC, and illustrate that the proposed controllers of Figs. 2 and 4 properly regulate P and Q to the desired values. Fig. 13(a) and (b) also shows that P and Q controllers exhibit some degree of coupling which is the inherent nature of the voltage-controlled strategy.

### B. Ride-Through Capability of DG Unit

Fig. 14 shows the ride-through capability of the system of Fig. 1, when subjected to a three-phase line-to-ground fault at the PCC. The fault is temporary and cleared 5 cycles after inception. Fig. 14(a) and (b) shows the PCC rms and instantaneous voltage (Phase A). The PCC voltage during the fault is below 0.5 p.u., however, since the fault period is less than 0.16 s, the voltage drop is within the ride-through capability of the DG unit [9] and the fault should not result in islanding or control change (i.e., $K_Q = 0$) of the DG unit.

Fig. 14(c) and (d) shows the converter output rms and instantaneous current. Fig. 14(c) and (d) indicates that the imposed control limits of Figs. 2 and 4 confine the converter current

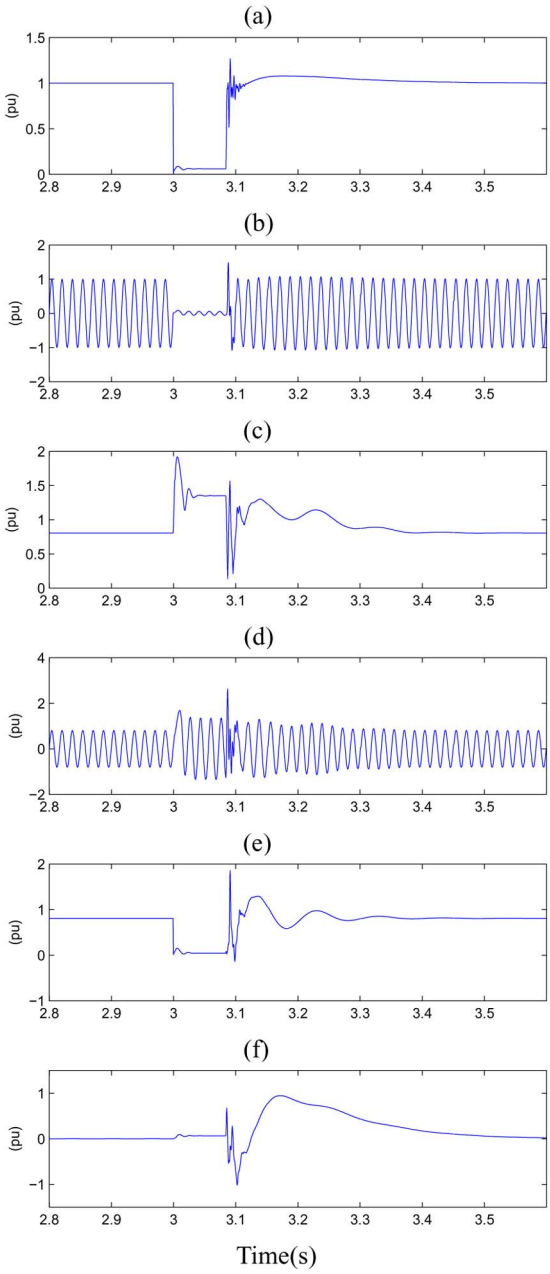


Fig. 14. Ride-through transients of the DG unit in a grid-connected mode due to a 5-cycle, three-phase, line-to-ground fault at PCC. (a) PCC rms voltage. (b) PCC instantaneous voltage (phase A). (c) Converter rms current. (d) Converter instantaneous current (phase A). (e) DG unit real power at PCC. (f) DG unit reactive power at PCC.

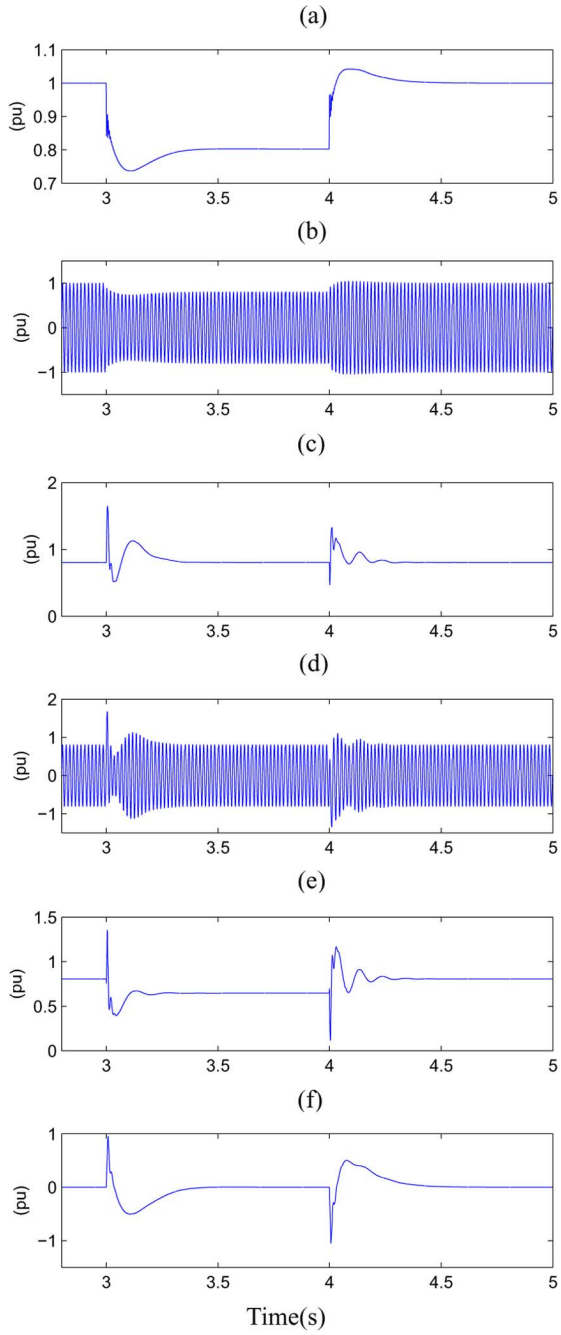


Fig. 15. Ride-through transients of the DG unit in a grid-connected mode due to a 1-s voltage drop (0.2 p.u.) of the grid source. (a) PCC rms voltage. (b) PCC instantaneous voltage (phase A). (c) Converter rms current. (d) Converter instantaneous current (phase A). (e) DG unit real power at PCC. (f) DG unit reactive power at PCC.

within 0 and 2 p.u. Without the limits, a maximum current of about 8 p.u. is encountered.

Fig. 14(e) and (f) shows instantaneous real- and reactive-power components of the DG unit at the PCC. Fig. 14(f) shows that the instantaneous reactive power undergoes a relatively large variation and slow dynamics after the fault is cleared. This is due to the PCC voltage feedback of Fig. 4 which is used to facilitate islanding detection. The reactive power transients settle down within 0.6 s which indicate that the PCC voltage feedback does not adversely affect the system transients, even under a three-phase ground fault conditions at PCC.

Fig. 15 shows the ride-through capability of the system of Fig. 1, due to a voltage drop (0.2 p.u.) for the period of 1.0 s at the grid source. Initially, the system is under a steady-state condition and the DG unit delivers 0.8/0.0 p.u. real/reactive power at PCC. The grid bus voltage drops 0.2 p.u., from 1.0 p.u. to 0.8 p.u., at $t = 3.0$ s. The abnormal condition lasts for one second from $t = 3.0$ s to $t = 4.0$ s.

Fig. 15(a) and (b) shows the PCC voltage. Fig. 15(a) shows that the PCC voltage drops below the permissible value of 0.88 p.u. as specified in Table I. However, since the period of voltage

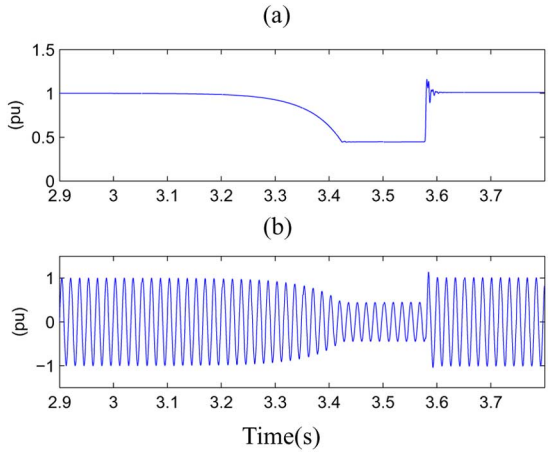


Fig. 16. Transients of the VSC terminal voltage during a preplanned islanding scenario of zero real- and reactive-power exchange with the grid. (a) PCC rms voltage. (b) PCC Instantaneous voltage (phase A).

drop is less than 2 s, the voltage abnormality is considered within the ride-through capability of the DG unit (Table I) and should not result in islanding or control change (i.e., $K_Q = 0$) of the DG unit [9]. Fig. 15(c) and (d) shows that the peak transient current of the converter is limited to 1.8 p.u.

Fig. 15(e) shows that during the time interval of 3.0 s to 4.0 s, power output of the VSC settles downs at a lower reference (i.e., 0.64 p.u.). This new reference is calculated by multiplying the original real power reference of Fig. 2 by the per unit value of PCC voltage when the PCC voltage drops to (and below) 0.88 p.u. The power reference is intentionally reduced during this time interval, however, the converter current reference is kept at the level prior to voltage drop at $t = 3.0$ s [Fig. 15(c)]. Motivation for reducing the power reference is to avoid over-current and prevent the over-current back-up protection to be activated, in case that the period of voltage drop lasts too long (e.g., beyond 1.8 s). Fig. 15(f) also shows that the reactive power undergoes transients immediately after a voltage change at $t = 3.0$ or $t = 4.0$ due to the PCC voltage feedback of Fig. 4. However, the transients settle down within 0.6 s.

### *C. Transition Capability From Grid-Connected to Islanded Mode*

Fig. 16 shows the capability of the system of Fig. 1 in terms of transition from a grid-connected mode to an islanded mode, due to a preplanned islanding scenario. Initially, the DG unit delivers 0.8/0.0 p.u. real/reactive power to the load at 1.0 p.u. PCC voltage. The RLC load is adjusted such that real- and reactive-power exchange with the grid is almost zero. At $t = 3$ s, a preplanned islanding event is imposed by opening switch $S_1$.

Since power exchange between the PCC and the grid prior to the islanding instant is insignificant, changes in the PCC voltage immediately after the islanding event ($t = 3.0$ s) are also insignificant [Fig. 16(a)]. However, due to the destabilizing effect of the VSC reactive power controller of Fig. 4, the PCC voltage gradually deviates from the initial value ($t = 3.0$ s). Change in the voltage is used as the islanding detection signal. Based on Table I:

- islanding detection process is initiated at $t = 3.3$ s corresponding to the PCC voltage of 0.88 p.u. and islanding detection is confirmed after 2 s delay;
- islanding detection process is initiated at $t = 3.42$ s, corresponding to the PCC voltage of 0.5 p.u. and islanding detection is confirmed after a 0.16-s delay.

Rapid PCC voltage drop from 0.88 ($t = 3.3$ s) to 0.5 p.u. ($t = 3.42$ s) s, Fig. 16(a), indicates that for the given scenario, 0.5 p.u. PCC voltage initiates islanding detection process and the islanding detection is confirmed after 0.16 s delay (i.e., at $t = 3.58$ s). Subsequent to the islanding detection confirmation, the reactive power control path of the controller of Fig. 4 is disabled by setting $K_Q = 0$, and the PCC voltage is restored to its normal value of 1.0 p.u., and the DG unit continues its operation in an autonomous mode. The total islanding detection time is 0.58 s.

Based on the voltage control scheme of Fig. 4, the PCC voltage should drop to and remain at zero for the time interval between 3.42 s and 3.58 s [Fig. 16(a)]. However, to improve dynamic performance of the autonomous system, after islanding detection initiation (e.g., at $t = 3.42$ s corresponding to the PCC voltage of 0.5 p.u.), when the PCC voltage drops to 0.48 p.u., it is maintained at 0.48 p.u. by disabling the positive feedback of Fig. 4 (by setting $K_V = 0$). When the positive feedback is disabled, the PCC voltage experiences a very slow rate of drop as shown in the time interval of 3.42 s to 3.58 s of Fig. 16. The rate of voltage drop depends on the amount of reactive power exchange between the PCC and the grid prior to the islanding event at $t = 3.0$ s. Without extending the islanding detection time, this voltage maintenance successfully prevents the PCC voltage from dropping to and remaining at zero for almost 0.16 s, which is an extreme operating condition for the system.

Other islanding scenarios, corresponding to different levels of real- and reactive-power exchange with the grid before the islanding event, were also studied. The studies show that the condition of zero real- and reactive-power exchange is the worst condition in terms of the required islanding detection time (0.58 s) and other islanding cases require less than 0.58 s to be detected. The proposed islanding detection method is robust since it 1) has no NDZ, and 2) is able to distinguish between the loss of the main grid and the grid disturbances.

Fig. 17 shows the transition capability of the system of Fig. 1, from a grid-connected mode to an islanded mode, due to an accidental islanding event which is initiated by a fault. Initially, the DG unit delivers 0.8/0.0 p.u. real/reactive power to the load at 1.0 p.u. PCC voltage. Real- and reactive-power exchange with the grid prior to the fault is almost zero. The grid is subjected to a three-phase to ground fault at the grid-side of $S_1$ at $t = 3$ s. Islanding occurs 5 cycles after the fault inception by opening $S_1$.

Fig. 17(a) and (b) shows the PCC rms and instantaneous voltages. Islanding detection process is initiated at $t = 3.0$ s since the PCC voltage immediately drops below 0.5 p.u. (Table I). The islanding detection confirmation time is after another 0.16 s or at $t = 3.16$ s. At $t = 3.083$ s $S_1$ opens, the fault is cleared and the grid continues its operation as an autonomous system. Immediately after opening $S_1$, the PCC voltage returns almost to

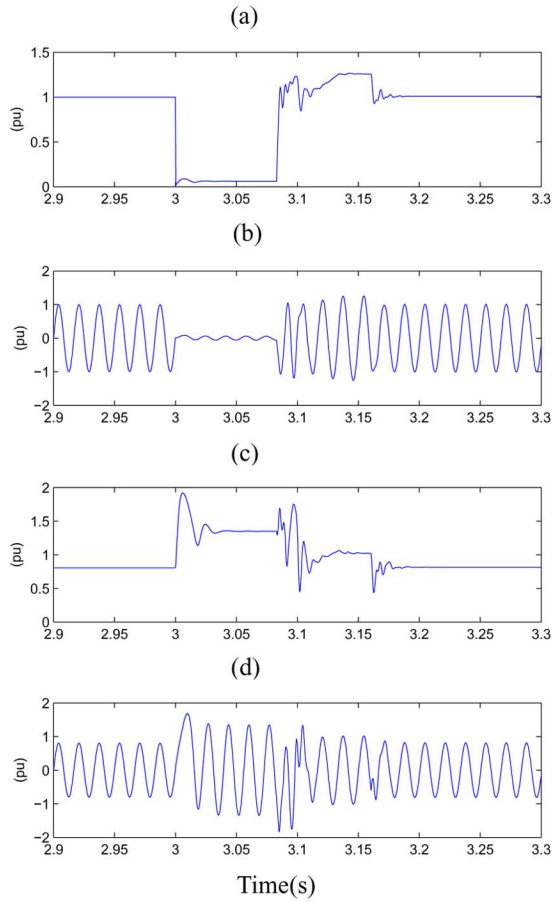


Fig. 17. Transients of the DG unit due to a three-phase fault at the grid-side of $S_1(t = 3.0\ \text{s})$. Islanding occurs after five cycles ($t = 3.083$ s). (a) PCC rms voltage. (b) PCC instantaneous voltage. (c) Converter rms current. (d) Converter instantaneous current.

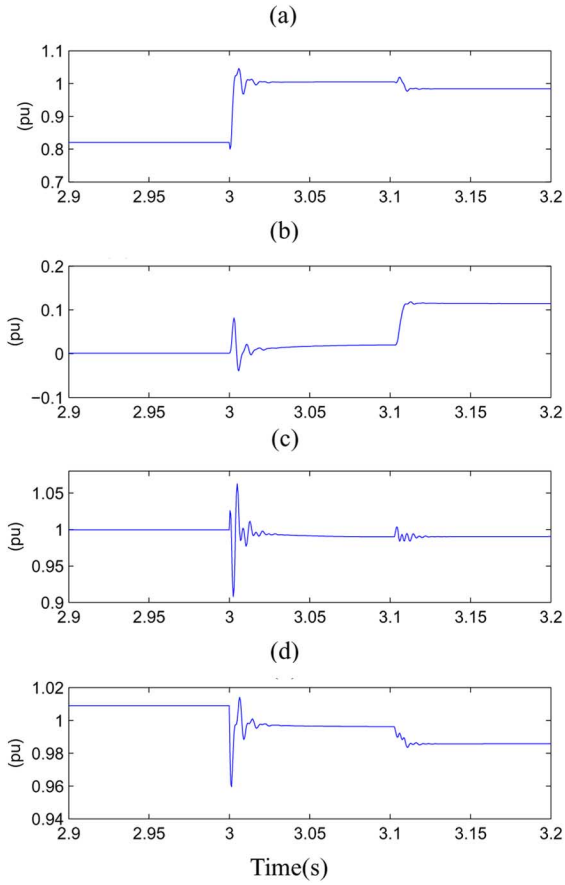


Fig. 18. Transient response of the DG unit to load changes ($\Delta P \approx 0.2$ p.u., $\Delta Q \approx 0.1$ p.u.) during the autonomous operation. (a) DG unit real power at PCC. (b) DG unit reactive power at PCC. (c) Estimated frequency at the PCC. (d) PCC rms voltage.

the prefault value since power exchange with the grid prior to the fault was insignificant. Then the PCC voltage begins to increase due to the positive feedback and the destabilizing voltage effect of the reactive power control of Fig. 4. It rises to 1.2 p.u. at $t = 3.13$ s [Fig. 17(a)], which can initiate another islanding detection process and the corresponding islanding detection confirmation after 0.16-s delay (Table I) (i.e., at $t = 3.29$ s). However, the initial islanding detection, which was activated at $t = 3.0$ s, is confirmed at $t = 3.16$ s, and disables the reactive power path of the controller of Fig. 4 ($K_Q = 0$). Therefore, the PCC voltage is restored to a value within the permissible range and the autonomous operation of the system continues. Fig. 17(c) and (d) shows the converter rms and instantaneous currents corresponding to phase A.

Similar to the case study of Fig. 16(a), the PCC voltage deviation of the case study of Fig. 17 is also limited for the period of $t = 3.13$ s to $t = 3.16$ s, by setting $K_V = 0$ (Fig. 4) when the PCC voltage intends to increase beyond 1.2 p.u. (i.e., at 1.22 p.u.).

### D. Autonomous Mode

Fig. 18 shows the transient response of the system of Fig. 1 to load changes during an autonomous mode of operation. Initially, the system is under a steady-state condition and the DG unit delivers 0.82/0.0 p.u. real/reactive power at 1.01 p.u. PCC voltage to the load. The system is subjected to two consecutive load changes. The load changes are imposed by changing R and L of the load (Fig. 1) from 1.25 p.u. and 0.8 p.u. to 1.0 p.u. and 0.74 p.u. (corresponding to step changes of 0.2 p.u. and 0.1 p.u. in real- and reactive-power) at $t = 3.0$ s and $t = 3.1$ s, respectively.

Fig. 18(a) and (b) shows variations in real- and reactive-power at the PCC, and indicates that the transients settle down within 0.05 s subsequent to the imposed disturbances. The PCC frequency is estimated by a PLL system and shown in Fig. 18(c), and indicates that the system steady-state frequency drops from 1 p.u. to 0.99 p.u. due to the real power increase, and does not noticeably change due to the reactive power change.

Fig. 18(d) shows that the steady-state PCC rms voltage drops 0.01 p.u., from 1.01 p.u. to 1.0 p.u., after real power increase, and drops 0.015 p.u., from 1.0 p.u. to 0.985 p.u., due to the reactive power change. Fig. 18(c) and (d) indicates that the real power change affects both the system frequency and the PCC voltage, while the reactive power change mainly affects the PCC voltage. Fig. 18(c) shows that there is a steady-state frequency drop after real power increase. This is a consequence of the $\omega$-P droop characteristic of the VSC. Similarly, steady-state PCC voltage drops after reactive power increase [Fig. 18(d)] due to the V-Q droop characteristic of the VSC.

## V. Conclusions

This paper presents a new control strategy for a VSC interfaced DG unit. The strategy controls the interface VSC as a voltage-controlled VSC (VC-VSC). The VC-VSC concept provides control over frequency and voltage through the VSC at its PCC and thus permits operation of the DG unit in both grid-connected and autonomous modes. The other features of the VC-VSC are:

- it provides ride-through capability for the DG unit under a grid-connected mode;
- it provides smooth transition capability between grid-connected and autonomous (islanded) modes subsequent to planned and accidental islanding events;
- it inherently includes an islanding detection capability without NDZ;
- it can provide current-limit capability for the converter during grid faults.

This paper also introduces a study system to demonstrate characteristics of the proposed VC-VSC strategy. An eigenanalysis is performed on the system to investigate dynamic stability of the system and select the proposed VC-VSC controller parameters. Time-domain simulation studies, in the PSCAD/EMTDC environment, are also carried out to 1) validate the eigenanalysis results and 2) evaluate transient performance of the VC-VSC strategy (e.g., ride-through capability, transition from grid-connected to islanded mode, and impact of load variations). The study results confirm merits of the proposed VSC control strategy.

## References

[1] T. Ackermann, G. Anderson, and L. Soder, "Distributed generation: A definition," *J. Elect. Power Syst. Res.*, no. 57, pp. 195–204, Jan. 2001.

[2] N. D. Hatziargyriou and A. P. S. Meliopoulos, "Distributed energy sources: Technical challenges," in *Proc. IEEE Power Eng. Soc. Winter Meeting*, 2002, vol. 2, pp. 1017–1022.

[3] J. Yao and D. Popovic, "Stability of a MV distribution network with electronically interfaced distributed generation," in *Proc. IEEE Mediterranean Electrotechnical Conf.*, 2004, vol. 3, pp. 975–978.

[4] C. Schauder and H. Mehta, "Vector analysis and control of advanced static VAR compensators," *Proc. Inst. Elect. Eng. C*, vol. 140, no. 4, pp. 299–306, Jul. 1993.

[5] R. H. Lasseter and P. Paigi, "Microgrid: A conceptual solution," in *Proc. IEEE Power Eng. Soc. Conf.*, 2004, pp. 4285–4290.

[6] F. Katiraei, M. R. Iravani, and P. Lehn, "Micro-grid autonomous operation during and subsequent to islanding process," *IEEE Trans. Power Del.*, vol. 20, no. 1, pp. 248–257, Jan. 2005.

[7] M. C. Chandorkar, D. M. Divan, and R. Adapa, "Control of parallel connected inverters in standalone ac supply systems," *IEEE Trans. Ind. Appl.*, vol. 29, no. 1, pp. 136–143, Jan./Feb. 1993.

[8] T. Funabashi, K. Koyanagi, and R. Yokoyama, "A review of islanding detection methods for distributed resources," presented at the Power Tech Conf., 2003.

[9] *Inverters, Converters, and Controllers for Use in Independent Power Systems*, UL Std. 1741, 2002.

[10] P. Kundur, *Power System Stability and Control*. New York: McGraw-Hill, 1994.

**Fang Gao** (S'05) received the B.Sc. and M.Sc. degrees in electrical engineering from Shanghai Jiao Tong University, Shanghai, China, in 1994 and 1997, respectively, and is currently pursuing the Ph.D. degree in electrical and computer engineering from the University of Toronto, Toronto, ON, Canada.

He was with Shanghai Municipal Electric Power Company, Shanghai, from 1997 to 2003. His research interests include power electronics and power system dynamics and control.

**M. Reza Iravani** (M'86–SM'02–F'03) received the B.Sc. degree in electrical engineering from Tehran Polytechnic University, Tehran, Iran, in 1976, and the M.Sc. and Ph.D. degrees in electrical engineering from the University of Manitoba, Winnipeg, MB, Canada, in 1981 and 1985, respectively.

Currently, he is a Professor at the University of Toronto, Toronto, ON, Canada. His research interests include power electronics and power system dynamics and control.